2014

Numerical Simulation of Single- and Dual-Media Thermocline Tanks for Energy Storage in Concentrating Solar Power Plants

C. Mira
Purdue University

S. M. Flueckiger
Purdue University

S V. Garimella
Purdue University, sureshg@purdue.edu

Available online at www.sciencedirect.com

SciVerse ScienceDirect

Energy Procedia 00 (2013) 000–000

Energy Procedia

www.elsevier.com/locate/procedia

SolarPACES 2013

Numerical Simulation of Single- and Dual-Media Thermocline Tanks for Energy Storage in Concentrating Solar Power Plants

C. Mira-Hernández, S.M. Flueckiger, S.V. Garimella*

Purdue University, 585 Purdue Mall, West Lafayette, IN 47905, USA

Abstract

A single molten-salt thermocline tank is a low-cost alternative to conventional multiple-tank systems for concentrating solar power thermal energy storage. Thermocline tanks are typically composed of molten salt and a filler material that provides sensible heat capacity at reduced cost; such tanks are referred to as a dual-media thermocline (DMT). However, inclusion of quartzite rock filler introduces the potential for mechanical ratcheting of the tank wall during thermal cycling. To avoid this potential thermomechanical mode of failure, the tank can be operated solely with molten salt, as a single-medium thermocline (SMT) tank. In the absence of a filler material to suppress formation of tank-scale convection eddies, the SMT tank may exhibit undesirable internal fluid flows in the tank cross-section. The performance of DMT and SMT tanks is compared under cyclic operation, assuming adiabatic external wall boundary conditions. A computational fluid dynamics model is used to solve for the spatial temperature and velocity distributions within the tank. For the DMT tank, a two-temperature model is used to account for the non-thermal equilibrium between the molten salt and the filler material, and Forchheimer's extension of Darcy's Law is added to the porous-medium formulation of the laminar momentum equation. The governing equations are solved numerically using a finite volume approach. For adiabatic external boundaries, the SMT tank yields a percentage point increase in the first and second law efficiencies relative to the DMT tank. Future work is needed to compare the thermocline tank designs with respect to capital cost and storage performance under non-adiabatic wall boundaries.

Selection and peer review by the scientific conference committee of SolarPACES 2013 under responsibility of PSE AG.

Keywords: thermocline, solar thermal energy, energy storage, molten salt

* Corresponding author. Tel.: +1-765-494-9095; fax: +1-765-494-0539.
E-mail address: sureshg@purdue.edu

Selection and peer review by the scientific conference committee of SolarPACES 2013 under responsibility of PSE AG.

1. Introduction

Concentrating solar power (CSP) is a promising and commercially viable technology for large-scale conversion of solar energy into electricity. In a CSP plant, focused sunlight is used to increase the thermal energy of a heat transfer fluid (HTF); the heated fluid is then utilized to produce steam that drives a Rankine cycle for electrical power generation. Reliance on direct solar radiation subjects CSP to the inherent intermittence of the insolation based on weather and cloud conditions, and requires cost-effective energy storage technologies to maintain steady power output, a key issue in the development and expansion of sustainable energy technologies [1]. The inclusion of thermal energy storage increases the performance of CSP plants by decoupling energy demand (for electricity generation) from solar energy availability [2–5].

Nomenclature

c_p	specific heat, J/kg-K
d	diameter of the thermocline tank, m
d_s	diameter of filler granules, m
E	energy, J
$\mathbf{e}$	unit vector
F	inertial coefficient
$\mathbf{g}$	gravitational acceleration, m/s^2
h	height of thermocline tank, m
h_i	volumetric interstitial convection coefficient, W/m^3-K
$\tilde{\mathbf{I}}$	identity tensor
K	permeability, m^2
$\dot{m}$	mass flow rate, kg/s
k	thermal conductivity, W/m-K
Nu_i	interstitial Nusselt number
p	pressure, Pa
Pr	Prandtl number
r	radial coordinate, m
Re	Reynolds number
$\tilde{\boldsymbol{S}}$	strain rate tensor, s^{-1}
t	time, s
t_0	half-cycle period, s
T	temperature, K
$\mathbf{u}$	velocity vector, m/s
v	traversal speed of the heat exchange region, m/s
u	velocity component, m/s
x	axial coordinate, m
X	exergy, J
Greek	
ε	porosity
η	efficiency
μ	viscosity, Pa-s
ρ	density, kg/m^3
$\tilde{\boldsymbol{\tau}}$	stress tensor, Pa
φ	solid fraction
Φ	viscous dissipation function, s^{-2}
Subscript	
c	low inlet discharge temperature
chg	charge process

dis	discharge process
eff	effective
h	high inlet charge temperature
in	inlet
l	molten salt
out	outlet
r	r-direction
s	solid filler
x	x-direction
θ	θ-direction
0	reference state
I	first law of thermodynamics
II	second law of thermodynamics

Thermocline tanks are sensible-heat thermal energy storage devices that have been applied in industrial and domestic energy conversion processes [6]. In a thermocline tank, both the cold and hot reserves of heat transfer fluid (HTF) are stored in a single tank in a manner that exploits buoyancy forces to promote thermal stratification. Isothermal hot and cold fluid regions become separated by a narrow region of temperature gradient, which is called the thermocline or heat-exchange region [2]. Due to their potential low cost relative to more conventional two-tank storage methods, molten-salt thermocline tanks are an attractive option for thermal energy storage in CSP systems [7,8]. In a dual-media thermocline (DMT) tank, a granulated material is added to the tank to reduce the amount of molten salt required to charge the system. In contrast, a single-medium thermocline (SMT) tank uses only molten salt.

DMT tanks are favored because they have economical and technical advantages over SMT tanks. The low-cost filler material replaces a large amount of the expensive molten salt, and requires only a marginal increase in total tank volume due to the slightly lower relative thermal capacity of the filler material. The filler material also acts as a porous-medium flow distributor that dampens secondary velocities in the tank cross-section that may destratify the hot and cold HTF regions. SMT tanks, in contrast, may be more vulnerable to non-uniform flow phenomena such as tank-scale mixing eddies. The importance of fluid distribution at the inlet is discussed in [9,10]. The thermal behavior of molten-salt DMT tanks has been studied via numerical models [8,11,12]; a few experimental studies have also been reported [8]. Extensive thermomechanical simulations of DMT tanks have been performed in the authors' group to quantify multi-dimensional thermal behavior inside the tank [13], performance under cyclic operation [14], structural stability of the tank wall [15], and system-level performance in conjunction with a CSP plant model [16].

One disadvantage of DMT tanks is possible mechanical failure by thermal ratcheting [15]. During cyclic operation, the tank wall and the internal filler material undergo differential thermal expansion and contraction. If the tank wall expands further than the filler material when heated, an annular gap may be formed into which the granulated unconsolidated filler material can redistribute. When the system is cycled and the wall is cooled, the settled filler granules would prevent complete contraction of the tank wall to its original dimensions, and generate a residual mechanical stress. If this stress is sufficient for the tank wall to yield, repeated wall expansions (or 'ratchets') may accumulate with each storage cycle until failure [15]. Thermal ratcheting does not occur in SMT tanks because of the absence of the filler material. There is also no risk of pipe system clogging by entrainment of the filler material into the molten-salt flow, and the design is simpler.

SMT tanks have been commonly used in power conversion technologies outside of CSP, such as industrial refrigeration systems [6] and domestic solar thermal devices [17]. In these low-temperature applications, water is used as the storage medium due to the high heat capacitance, availability, and low cost. Water tanks with thermal stratification are a mature technology; analytical, numerical and experimental studies have been previously reported [18–21]. Molten-salt SMT tanks for CSP applications, however, remain unexplored.

The present work assesses the comparative performance and thermal behavior of molten-salt DMT and SMT tanks under cyclic thermal operation and adiabatic external boundary conditions.

2. Numerical modeling

2.1. Problem description

The numerical analysis considers a thermocline tank with a discharge power of 25 MWt, and 12-hour charge/discharge processes from 600 °C and 300 °C hot and cold HTF sources, respectively. The tank is sized to store 12 h of thermal energy with an overdesign capacity of 1.5 h. A tank overdesign is necessary for simultaneous containment of the desired thermal energy (at high temperature) and the underlying heat-exchange region composed of HTF at cold and transitional temperatures. The molten salt is a commercial eutectic mixture of sodium nitrate (60 wt.%) and potassium nitrate (40 wt.%) that solidifies at 221 °C. The temperature-dependent molten salt physical properties are calculated using the following curve fits derived from experimental data (temperature in Celsius) [22]:

$$\text{Density (kg/m}^3\text{)}: \ \rho_l(T_l) = 2090 - 0.636T_l \tag{1}$$

$$\text{Viscosity (mPa-s)}: \ \mu_l(T_l) = 22.714 - 0.120T_l + 2.281\times10^{-4}T_l^{\,2} - 1.474\times10^{-7}T_l^{\,3} \tag{2}$$

$$\text{Thermal conductivity (W/m-K)}: \ k_l(T_l) = 0.443 + 1.9\times10^{-4}T_l \tag{3}$$

The specific capacity of the molten salt is relatively constant in the operating temperature range; a mean value over this range of 1520 kJ/kg-K is used. The required mass flow rate of molten salt is 54.8 kg/s at the prescribed discharge power. The DMT and SMT tanks are sized based on the desired thermal capacity and discharge power. The height of the tank is set to 12 m for both cases, as a practicable value based on previous reports [23]. Fig 1 schematically illustrates both units.

The diameter of the SMT tank is 12.85 m with a molten salt volume of 1556 m^3. The diameter of the DMT tank is 14 m and the total volume of the filler bed is 1847 m^3. The filler inside of the DMT tank is quartzite rock with a mean particle diameter of 15 mm and porosity of 0.22 [8]. The amount of salt inside the DMT tank is therefore 406 m^3. The properties of the quartzite rock are treated as constant, with a specific heat of 830 J/kg-K, a density of 2500 kg/m^3 and a thermal conductivity of 5 W/m-K [13,24].

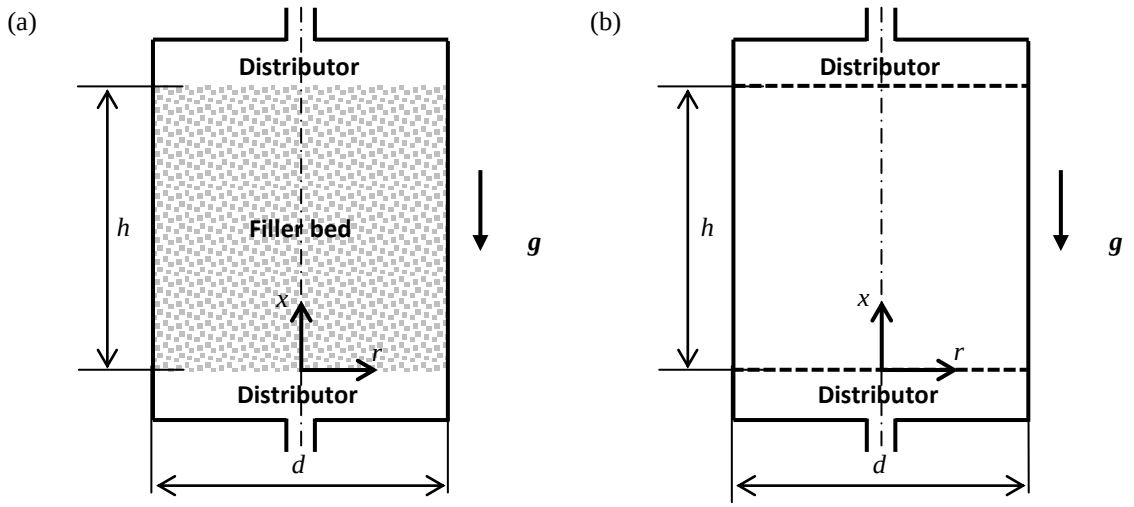

Fig 1. Schematic illustrations of (a) a dual-media and (b) a single-medium thermocline tank.

The cyclical operation of both systems is identical. During the charge process, hot molten salt (carrying energy from the solar field) enters at the top of the tank while cold fluid exits at the bottom to be routed for heating to the solar field. During the discharge process, cold fluid from the power block enters at the bottom of the tank while hot fluid exits from the top (delivering energy for steam generation). In an actual thermocline tank, distributors must be used to promote uniform, unidirectional flow and curtail mixing of hot and cold fluid. For the present model, ideal distribution is assumed, and distributors are omitted from the model geometry; uniform flow conditions are imposed at the inlet and outlet of the main thermal energy storage region. The charge and discharge processes each last 12 h. The total cycle has a duration of 24 h and does not include any dwell-time without flow.

2.2. Governing equations and boundary conditions

The thermal behavior of a thermocline tank is governed by mass, momentum, and energy conservation principles. Governing equations are formulated for both the DMT tank and the SMT tank. These equations are described in detail here for the DMT tank, as equations for the SMT tank can be obtained from straightforward simplification of the DMT model.

The motion of the molten salt inside the thermocline tank obeys the mass and momentum conservation principles as expressed in the following laminar flow equations. Darcy's and Forchheimer's terms are included to account for viscous and inertial momentum dissipation in the porous bed. The equations are stated in terms of the seepage velocity:

$$\frac{\partial(\varepsilon\rho_l)}{\partial t}+\nabla\cdot(\rho_l\mathbf{u})=0 \tag{4}$$

$$\frac{\partial(\rho_l\mathbf{u})}{\partial t}+\nabla\cdot\left(\rho_l\frac{\mathbf{uu}}{\varepsilon}\right)=-\varepsilon\nabla p+\nabla\cdot\tilde{\boldsymbol{\tau}}+\varepsilon\rho_l\mathbf{g}+\varepsilon\left(\frac{\mu}{K}\mathbf{u}+\frac{F}{\sqrt{K}}\rho_l|\mathbf{u}|\mathbf{u}\right) \tag{5}$$

where the stress tensor is defined as $\tilde{\boldsymbol{\tau}}=\mu(2\tilde{\mathbf{S}}-(2/3)\mathrm{tr}(\tilde{\mathbf{S}})\tilde{\mathbf{I}})$ with the strain rate tensor $\tilde{\mathbf{S}}=1/2\,(\nabla\mathbf{u}+(\nabla\mathbf{u})^T)$. The spatial gradient in cylindrical coordinates is $\nabla=\mathbf{e}_r(\partial/\partial r)+\mathbf{e}_\theta(1/r)(\partial/\partial\theta)+\mathbf{e}_x(\partial/\partial x)$. Fluid flow is assumed to be two-dimensional axisymmetric, eliminating all angular functional dependencies. Relations from the literature are used for the permeability, evaluated as $K=d_s^2\varepsilon^3/175(1-\varepsilon)$ [25], and for the inertial coefficient, evaluated as $F=1.75/\sqrt{150\varepsilon}$ [26].

In the DMT tank case, the molten salt exchanges thermal energy with the filler bed. Hence, there is no thermal equilibrium between both phases and separate energy equations are required for each:

$$\frac{\partial\left(\varepsilon\rho_l c_{p,l}(T_l-T_c)\right)}{\partial t}+\nabla\cdot\left(\rho_l\mathbf{u}c_{p,l}(T_l-T_c)\right)=\nabla\cdot\left(k_{eff}\nabla T_l\right)+\mu\Phi+h_i(T_s-T_l) \tag{6}$$

$$\frac{\partial\left((1-\varepsilon)\rho_s c_{p,s}(T_s-T_c)\right)}{\partial t}=-h_i(T_s-T_l) \tag{7}$$

The energy equations are coupled by the volumetric heat transfer rate between the solid and liquid phases due to interstitial convection. The interstitial heat transfer coefficient is calculated as [27]:

$$\mathrm{Nu}_i=6(1-\varepsilon)\left(2+1.1\mathrm{Re}^{0.6}\,\mathrm{Pr}^{1/3}\right) \tag{8}$$

The filler bed forms an unconsolidated porous medium with minimal contact area between particles. Hence, heat conduction between the solid particles is assumed to be negligible. However, an effective thermal conductivity is

included in the liquid-phase energy equation to account for the additional thermal diffusion in the porous medium. The effective thermal conductivity of the solid-liquid mixture is [28]:

$$k_{eff} = k_l \frac{1 + 2\beta\phi + \left(2\beta^3 - 0.1\beta\right)\phi^2 + \phi^3 0.05 e^{4.5\beta}}{1 - \beta\phi} \tag{9}$$

where ϕ=1-ε, and $\beta=(k_s-k_l)/(k_s+2k_l)$.

The simplified form of the governing equations used for the SMT tank model can be obtained from the expressions above setting the porosity to unity and considering an infinite permeability. In this case, the mass and momentum conservation can be expressed as follows:

$$\frac{\partial \rho_l}{\partial t} + \nabla \cdot \left(\rho_l \mathbf{u}\right) = 0 \tag{10}$$

$$\frac{\partial \left(\rho_l \mathbf{u}\right)}{\partial t} + \nabla \cdot \left(\rho_l \mathbf{u}\mathbf{u}\right) = -\nabla p + \nabla \cdot \tilde{\boldsymbol{\tau}} + \rho_l \mathbf{g} \tag{11}$$

Only one energy equation is required for the SMT tank. The effective thermal conductivity is equal to the thermal conductivity of the molten salt.

$$\frac{\partial \left(\rho_l c_{p,l} T_l\right)}{\partial t} + \nabla \cdot \left(\rho_l \mathbf{u} c_{p,l} T_l\right) = \nabla \cdot \left(k_l \nabla T_l\right) + \mu\Phi \tag{12}$$

The boundary conditions applied depend on the phase in the cycle of operation. The tank side wall is modeled as non-slip and adiabatic during all stages of the cycle. During the charge process, when hot molten salt enters at the top of the tank, the top of the tank is specified to be an inlet with uniform velocity and temperature T_h. Cold molten salt exits the tank at the bottom where outflow conditions are imposed:

$$T\big|_{x=h} = T_h \qquad u_x\big|_{x=h} = u_h \qquad \left.\frac{\partial T}{\partial x}\right|_{x=0} = \left.\frac{\partial u_x}{\partial x}\right|_{x=0} = \left.\frac{\partial u_r}{\partial x}\right|_{x=0} = 0 \tag{13}$$

During the discharge process the flow is reversed and cold molten salt enters at the bottom of the tank with uniform velocity and temperature T_c. The top wall is modeled as an outlet:

$$T\big|_{x=0} = T_c \qquad u_x\big|_{x=0} = u_c \qquad \left.\frac{\partial T}{\partial x}\right|_{x=h} = \left.\frac{\partial u_x}{\partial x}\right|_{x=h} = \left.\frac{\partial u_r}{\partial x}\right|_{x=h} = 0 \tag{14}$$

2.3. Solution procedure

The governing equations are numerically solved using the finite volume method using the commercial computational fluid dynamics software FLUENT [29]. The two-dimensional domain is discretized into a structured mesh composed of rectangular cells. Each of these cells is treated as a control volume for which the balance equations of conserved quantities are written as algebraic expressions; in this way, the solution method assures global conservation of mass, energy and momentum. Flow variables may be interpolated at the cell faces with different discretization schemes. For the present study, a second-order upwind scheme is used for spatial discretization of convective fluxes and a body force-weighted scheme is used for spatial discretization of the

pressure. Transient discretization is performed with a first-order implicit formulation. Pressure-velocity coupling is accomplished with the pressure implicit with splitting of operators (PISO) algorithm [30]. Experimental validation of this model was demonstrated in [13] with a simulation of a 2.3 MWh DMT tank previously built by Sandia National Laboratories [8].

For both thermocline tank geometries the mesh size is $\Delta r = 0.005\,d$ in the radial direction and $\Delta x = 0.01\,h$ in the axial direction. The time step for the simulation of the DMT tank is $\Delta t = 6$ s; mesh independence was previously verified by Yang and Garimella [13]. For the SMT tank, a smaller time step of $\Delta t = 0.6$ s is required to achieve converged solutions. In the SMT tank, momentum dissipation mechanisms are reduced due to the lack of a porous filler, resulting in the development of a hydrodynamic boundary layer along the interior tank wall, in contrast to the DMT tank. A grid check was performed for the SMT tank using constant fluid properties to verify that the applied mesh size successfully resolved the layer. As an initial condition for both tanks, the temperature of the upper half of the tank is set to 600 °C and the lower half of the tank to 300 °C. Convergence to periodicity is achieved after the simulation of seven cycles, each one consisting of a 12 h charge process and a 12 h discharge process. The performance of the SMT tank is compared with that of the DMT tank under periodic response conditions.

3. Results and discussion

3.1. Temperature field

Profiles of the molten-salt temperature along the tank axis during charge and discharge processes for the DMT and SMT tanks are plotted in Fig 2. At each time, three zones can be identified: a zone of uniform low temperature, a zone with notable temperature gradient (heat-exchange region), and a zone of uniform high temperature. The heat-exchange region moves downward during the charge (from right to left in the plot) and upward during the discharge process (from left to right in the plot). The speed of the heat-exchange region is nearly equal in both thermocline units: 0.249 mm/s in the DMT tank and 0.248 mm/s in the SMT tank. These results are in good agreement with the expression for heat-exchange region velocity proposed by Yang and Garimella [13]:

$$v = u_h \frac{\rho_{l,h} c_{p,l}}{\varepsilon \rho_{l,h} c_{p,l} + (1-\varepsilon)\rho_s c_{p,s}} \tag{15}$$

The equation is evaluated using a porosity of 1 for the SMT tank, in which case the speed of the heat-exchange region equals the inlet velocity.

In an ideal adiabatic thermocline tank, a heat-exchange zone should not occur, and all of the stored molten salt should be retrieved at the high temperature, without energy and exergy losses. In practice, however, a region of temperature gradient develops due to thermal diffusion in the fluid. The length of this zone is a measure of the thermal stratification inside the tank; as the length increases (poor stratification), the quality of the energy stored in the tank decreases. In the present study, the length of the heat-exchange zone is defined as the region that contains 98% of the overall temperature change, namely the region in which: $0.01 \leq (T - T_c)/(T_h - T_c) \leq 0.99$. As seen in Fig 2 from the slopes of the temperature curves, thermal diffusion occurs more readily in the DMT tank. The length of the heat-exchange zone in the DMT tank is 3.29 m while in the SMT tank is 2.14 m. This is due to the higher thermal conductivity of the filler material, which causes a higher effective thermal diffusivity (both the filler material and molten salt have similar heat capacity).

It should also be noted that the "S"-shaped temperature profiles in Fig 2 are not symmetric about the median temperature of 450 °C. The heat-exchange region tends to be stretched in a particular direction depending on the cycle direction. For instance, at the middle of the discharge process, $t = 18$ h, the heat-exchange region is larger on the hot molten-salt side. The situation is reversed halfway through the charge process, at $t = 6$ h, and the heat-exchange region is larger on the cold molten-salt side. This phenomenon is related to the changes in the flow conditions at the ports during the transitions between the discharge and charge processes. At the end of the discharge process a portion of the salt in the heat-exchange region is delivered to the power system; when the charge process begins, fresh hot molten salt enters at the top of the tank. In this way, the heat-exchange region becomes

shorter on one side due to the initial temperature discontinuity at the tank inlet. The effect is more pronounced for the DMT tank in which thermal diffusion is higher.

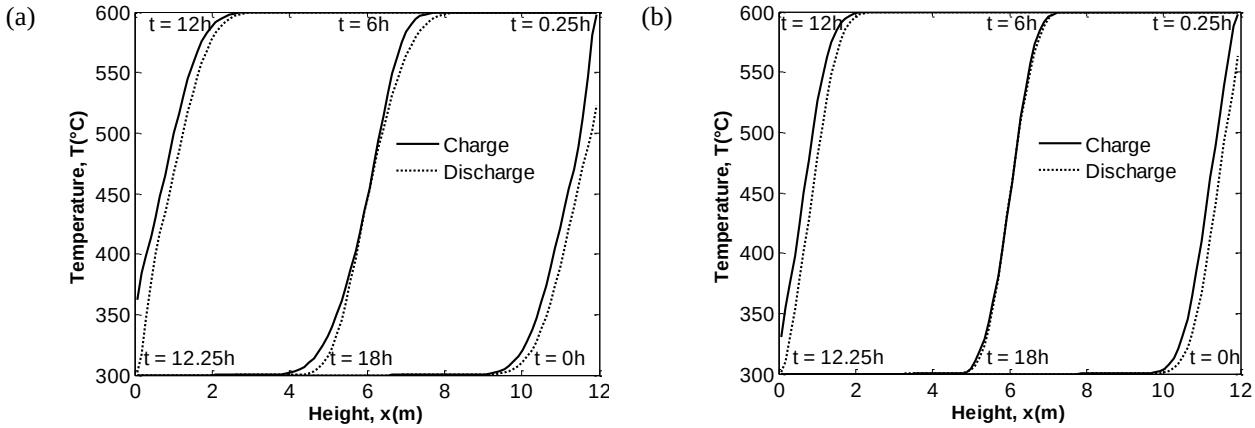

Fig 2. Molten-salt temperature along the axis of the (a) dual-media thermocline tank and (b) single-medium thermocline tank.

3.2. Outflow temperature history and discharge efficiency

The temporal molten-salt outflow temperatures during the discharge process for the DMT and SMT tanks are plotted in Fig 3. At the beginning of the discharge process the outflow temperature is equal to the inlet charge temperature of 600 °C, and it remains constant during most of the process. At some point, the outflow temperature begins to decrease and reaches its lowest value at the end of the discharge process. The outflow temperature drops by 77.0 K in the DMT tank and by 36.3 K in the SMT tank. The smaller temperature drop exhibited by the SMT tank is preferable as more high-temperature molten salt is delivered to the power block steam generators. As such, more electricity will then be delivered to the grid.

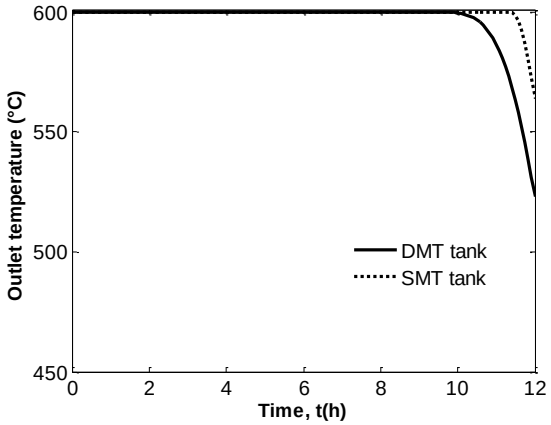

Fig 3 Outflow temperature history for dual-media and single-medium thermocline tanks.

The outflow temperature history during the discharge process is used to assess the performance of the thermocline tank as a thermal energy storage system. In an ideal adiabatic thermocline tank, the molten salt is recovered at the same temperature at which it is stored; however, due to the heat exchange with the cold molten salt, a certain amount of molten salt is delivered at lower temperature, and it is not possible to completely recover the energy and exergy that are initially stored. First and second law efficiencies compare the energy and exergy

delivered during the discharge process with the stored values during the charge process. These efficiencies are defined as follows:

$$\eta_I = \frac{E_{out,dis}}{E_{in,chg}} = \frac{\int_0^{t_0} \dot{m}_{out,dis}\left(T_{out} - T_c\right)dt}{\dot{m}_{in,chg}\left(T_h - T_c\right)t_0} \tag{16}$$

$$\eta_{II} = \frac{X_{out,dis}}{X_{in,chg}} = \frac{\int_0^{t_0} \dot{m}_{out,dis}\left[\left(T_{out} - T_c\right) - T_o \ln\left(T_{out}/T_c\right)\right]dt}{\dot{m}_{in,chg}\left[\left(T_h - T_c\right) - T_o \ln\left(T_h/T_c\right)\right]t_0} \tag{17}$$

The first law efficiency of the DMT tank is 98.89% while its second law efficiency is 98.75%. For the SMT tank, these values are 99.81% and 99.78% respectively. Given these high efficiencies, both thermocline tank types are suitable as a thermal energy storage device for CSP plants. It should be noted, however, that the SMT tank could be more sensitive to flow disturbances. For instance, the development of a hydrodynamic boundary layer along the SMT tank wall, illustrated in Fig 4, can induce flow non-uniformities. This behavior, especially when exacerbated by the presence of external heat losses, is under investigation in ongoing work. It should also be noted that the material cost of the quartzite rock is less than that of molten salt, and thus, an economic study is also needed to compare the DMT tank with the non-ratcheting SMT tank.

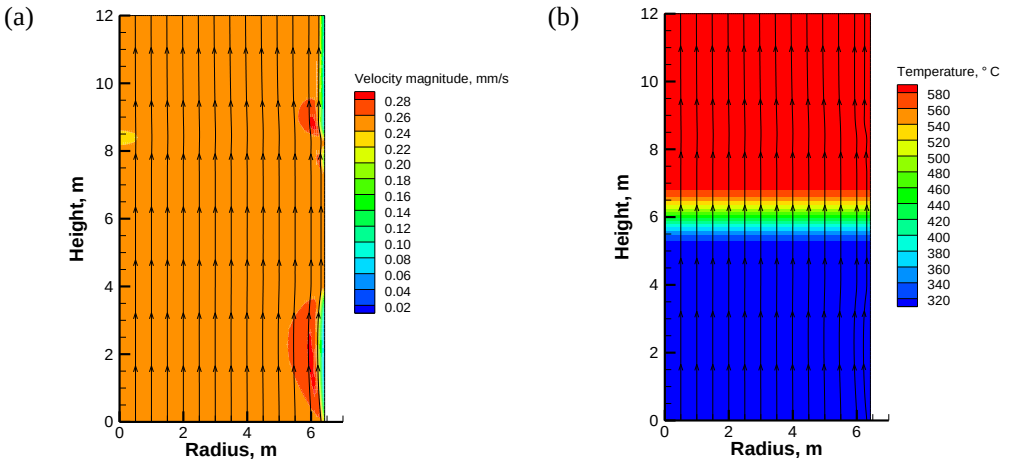

Fig 4. Single-medium thermocline tank: (a) velocity contours and (b) temperature contours halfway through the discharge process (t = 18 h).

4. Conclusion

Two types of molten-salt thermocline tanks for a thermal energy storage system are explored through numerical simulation, namely, a conventional DMT tank with quartzite rock as filler material, and a SMT tank. The thermal performance under cyclic operation and adiabatic external boundary conditions is comparatively assessed using temperature distribution inside the thermocline tank, outflow temperature history, and first and second law efficiencies as metrics. Greater thermal diffusion is observed in the DMT tank, which elongates the heat-exchange region along the height of the porous region. This is expected due to the higher thermal diffusivity of the quartzite rock, and is the main cause of the differences (outflow temperature history and storage cycle efficiency) observed in the performance of the two kinds of thermocline tanks. Under the adiabatic conditions of operation considered in this study both units have high thermal performance, with slightly higher First- and Second-Law efficiencies for the SMT tank.

Acknowledgements

This paper is based upon work supported in part under the US-India Partnership to Advance Clean Energy-Research (PACE-R) for the Solar Energy Research Institute for India and the United States (SERIIUS), funded jointly by the U.S. Department of Energy (Office of Science, Office of Basic Energy Sciences, and Energy Efficiency and Renewable Energy, Solar Energy Technology Program, under Subcontract DE-AC36-08GO28308 to the National Renewable Energy Laboratory, Golden, Colorado) and the Government of India, through the Department of Science and Technology under Subcontract IUSSTF/JCERDC-SERIIUS/2012 dated 22nd Nov. 2012.

References

[1] Ibrahim H, Ilinca A, Perron J. Energy storage systems—Characteristics and comparisons. Renewable and Sustainable Energy Reviews 2008;12:1221–50.
[2] Gil A, Medrano M, Martorell I, Lázaro A, Dolado P, Zalba B, et al. State of the art on high temperature thermal energy storage for power generation. Part 1—Concepts, materials and modellization. Renewable and Sustainable Energy Reviews 2010;14:31–55.
[3] Tamme R, Laing D, Steinmann W-D. Advanced thermal energy storage technology for parabolic trough. Journal of Solar Energy Engineering 2004;126:794–800.
[4] Luzzi A, Lovegrove K, Filippi E, Fricker H, Schmitz-Goeb M, Chandapillai M, et al. Techno-economic analysis of a 10 MWe solar thermal power plant using ammonia-based thermochemical energy storage. Solar Energy 1999;66:91–101.
[5] Herrmann U, Kelly B, Price H. Two-tank molten salt storage for parabolic trough solar power plants. Energy 2004;29:883–93.
[6] Dincer I. On thermal energy storage systems and applications in buildings. Energy and Buildings 2002;34:377–88.
[7] Kearney D, Herrmann U, Nava P, Kelly B, Mahoney R, Pacheco J, et al. Assessment of a Molten Salt Heat Transfer Fluid in a Parabolic Trough Solar Field. Journal of Solar Energy Engineering 2003;125:170.
[8] Pacheco JE, Showalter SK, Kolb WJ. Development of a molten-salt thermocline thermal storage system for parabolic trough plants. Journal of Solar Energy Engineering 2002;124:153.
[9] Zurigat Y, Liche P, Ghajar A. Influence of inlet geometry on mixing in thermocline thermal energy storage. International Journal of Heat and Mass Transfer 1991;34:115–25.
[10] Chung JD, Cho SH, Tae CS, Yoo H. The effect of diffuser configuration on thermal stratification in a rectangular storage tank. Renewable Energy 2008;33:2236–45.
[11] Li P, Van Lew J, Karaki W, Chan C, Stephens J, Wang Q. Generalized charts of energy storage effectiveness for thermocline heat storage tank design and calibration. Solar Energy 2011;85:2130–43.
[12] Arahal MR, Cirre CM, Berenguel M. Serial grey-box model of a stratified thermal tank for hierarchical control of a solar plant. Solar Energy 2008;82:441–51.
[13] Yang Z, Garimella SV. Thermal analysis of solar thermal energy storage in a molten-salt thermocline. Solar Energy 2010;84:974–85.
[14] Yang Z, Garimella SV. Cyclic operation of molten-salt thermal energy storage in thermoclines for solar power plants. Applied Energy 2013;103:256–65.
[15] Flueckiger SM, Yang Z, Garimella SV. Thermomechanical simulation of the Solar One thermocline storage tank. Journal of Solar Energy Engineering 2012;134:041014.
[16] Flueckiger SM, Iverson BD, Garimella SV, Pacheco JE. System-level simulation of a solar power tower plant with thermocline thermal energy storage. Applied Energy 2014;113:86-96.
[17] Abdoly M, Rapp D. Theoretical and experimental studies of stratified thermocline storage of hot water. Energy Conversion and Management 1982;22:275–85.
[18] Yoo H, Pak E. Theoretical model of the charging process for stratified thermal storage tanks. Solar Energy 1993;51:513–9.
[19] Han YM, Wang RZ, Dai YJ. Thermal stratification within the water tank. Renewable and Sustainable Energy Reviews 2009;13:1014–26.
[20] Bahnfleth WP, Song J. Constant flow rate charging characteristics of a full-scale stratified chilled water storage tank with double-ring slotted pipe diffusers. Applied Thermal Engineering 2005;25:3067–82.
[21] Al-Najem N. Degradation of a stratified thermocline in a solar storage tank. International Journal of Energy Research 1993;17:183–91.
[22] Pacheco JE, Ralph ME, Chavez JM, Dunkin SR, Rush EE, Ghanbari CM, et al. Results of molten salt panel and component experiments for solar central receivers: cold fill, freeze/thaw, thermal cycling and shock, and instrumentation. Sandia National Laboratories, Report No SAND94-2525 1995.
[23] Solar thermocline storage systems. EPRI 1019581 2010.
[24] Côté J, Konrad J. A generalized thermal conductivity model for soils and construction materials. Canadian Geotechnical Journal 2005;458:443–58.
[25] Beckermann C, Viskanta R. Natural convection solid/liquid phase change in porous media. Int. J. of Heat and Mass Transfer 1988;31:35–46.
[26] Krishnan S, Murthy JY, Garimella SV. A two-temperature model for the analysis of passive thermal control systems. Journal of Heat Transfer 2004;126:628–37.
[27] Wakao N, Kaguei S. Heat and mass transfer in packed beds. New York: Gordon and Breach Science Publishers; 1982.
[28] Gonzo EE. Estimating correlations for the effective thermal conductivity of granular materials. Chemical Engineering J. 2002;90:299–302.
[29] ANSYS. Fluent 14.5.0 2011.
[30] Issa R. Solution of the implicitly discretised fluid flow equations by operator-splitting. Journal of Computational Physics 1986;65:40–65.